ELSEVIER

Journal of Nuclear Materials 246 (1997) 158–164

journal of nuclear materials

# The effects of oxidation on the thermal conductivity of (U, M)$O_2$ pellets (M = Gd and/or simulated soluble FPs)

Masaki Amaya *, Mutsumi Hirai

*Nippon Nuclear Fuel Development Co., Ltd., 2163, Narita-cho, Oarai-machi, Higashi-ibaraki-gun, Ibaraki-ken 311-13, Japan*

Received 15 February 1997; accepted 29 April 1997

**Abstract**

10 wt% $Gd_2O_3$ doped $UO_{2+x}$ samples with $x$ being between 0 and 0.15 and simulated soluble FP doped $UO_{2+x}$ (simulated burnups: 30 and 60 GWd/tU), with $x$ between 0 and 0.02, were prepared with an oxidation method. Sample thermal diffusivities were measured by using a laser flash method from 300 to 1400 K and sample thermal conductivities were evaluated by multiplying the thermal diffusivities by the sample densities and the specific heat capacities derived from the literature. The thermal conductivities of (U, M)$O_{2+x}$ (M = Gd and/or simulated soluble FPs) decreased with increasing hyperstoichiometry and they were expressed as a function of hyperstoichiometry and the concentration of impurities such as $Gd^{3+}$ and FP ions. © 1997 Elsevier Science B.V.

## 1. Introduction

In the event of a fuel rod failure in a BWR, $UO_2$ fuel pellets react with high temperature and high pressure steam which enters the fuel rod and they are oxidized. The O/U ratio of the $UO_2$ pellets changes from 2 to about 2.1 [1] in the initial leak stage. Thermal conductivity is one of the most important thermal properties to evaluate the temperature in the oxidized pellets, which may control the distribution of FPs in the pellets.

Thermal conductivities of unirradiated $UO_{2+x}$ pellets have been measured by several groups [2–6]. We compared these data, having nearly the same sample densities, and found that considerable disagreement was noted between the published data for O/U ratios above 2.05 and there is few thermal conductivity data for composition $O/U > 2.1$. We have measured the thermal conductivities of $UO_{2+x}$ pellets [7] paying attention to sample characteristics and our results suggested that the disagreement among the literature data was mainly due to the differences in the sample density evaluation. We also expressed the thermal conductivities of $UO_{2+x}$ pellets in the composition range from O/U = 2.00 to 2.15 by using the deviation from the stoichiometry, $x$, applying Klemens' model based on quantum theory [8,9].

On the other hand, there are few studies on thermal conductivities of impurity-doped $UO_{2+x}$ pellets. Recently, thermal conductivities of unirradiated hyperstoichiometric SIMFUEL were measured by Lucuta et al. [6] in the composition range from 2.000 to 2.084. They determined the sample O/M ratios by using the relationship of oxygen potentials for pure $UO_{2+x}$. However, since the oxygen potentials for SIMFUEL are changed compared with those of pure $UO_{2+x}$ [10], as they also pointed out, it is possible that the O/M ratios of Lucuta et al.'s hyperstoichiometric SIMFUEL samples deviated from the accurate ones. And they used the theoretical densities of stoichiometric samples for hyperstoichiometric ones. It is not easy to evaluate the theoretical density changes of their oxidized SIMFUEL samples because the composition of metallic inclusions were scattered [11]. Our estimation results show that the thermal conductivity decrease due to oxidation was at least about 3% overestimated at O/M = 2.08 and the overestimation grows larger as increasing O/M ratios due to the differences in the sample density evaluation. From the view points of the fuel performance analysis, this overestimation causes about 50 K rise in fuel center temperature

* Corresponding author. Tel.: +81-29 266 2131; fax: +81-29 266 2589; e-mail: amaya@nfd.co.jp.


*PII* S0022-3115(97)00105-0

Table 1
Sample preparation conditions of 10 wt% $Gd_2O_3$ doped $UO_{2+x}$

| O/M ratio | Starting material | Preparation conditions |
|---|---|---|
| 2.00 | (green pellet) | sintered for 4 h at 2023 K in $N_2$–8%$H_2$–$H_2O$ (dew point: room temperature) |
| 2.06 | (U, Gd)$O_2$ pellet | oxidized for 1 h at 923 K in Ar ($P_{O_2} < 2 \times 10^{-2}$ Pa), annealed for 2 h at 1273 K in vacuum ($< 1 \times 10^{-4}$ Pa) |
| 2.08 | (U, Gd)$O_2$ pellet | oxidized for 10 h at 1223 K in Ar–13%$H_2O$ |
| 2.11 | (U, Gd)$O_2$ pellet | oxidized for 5 h at 1273 K in Ar–$H_2O$ (dew point: room temperature) |
| 2.15 | (U, Gd)$O_2$ pellet | oxidized for 5 h at 1273 K in Ar–13%$H_2O$ |

Table 2
Sample preparation conditions of simulated soluble FP-doped $UO_{2+x}$ (simulated burnups: 30 and 60 GW d/t U)

| O/M ratio | Starting material | Preparation conditions |
|---|---|---|
| 2.00 | (green pellet [a]) | sintered for 4 h at 2023 K in $N_2$–8%$H_2$–$H_2O$ (dew point: room temperature) |
| 2.02 | (U, FP [a])$O_2$ pellet | oxidized for 15 h at 1273 K in Ar–13%$H_2O$ |

| Concentration of the additives (wt%) | | | | | | |
|---|---|---|---|---|---|---|
| Simulated burnup (GW d/t U) | SrO | $Y_2O_3$ | $ZrO_2$ | $LaO_2$ | $CeO_2$ | $Nd_2O_3$ |
| 30 | 0.090 | 0.050 | 0.403 | 0.118 | 0.407 | 0.397 |
| 60 | 0.142 | 0.080 | 0.717 | 0.227 | 0.750 | 0.809 |

[a] For the concentration of the additives, see the lower half of this table.

during irradiation in a commercial reactor. This temperature difference affects the fuel behavior to a considerable degree.

In this paper, we prepared the (U, simulated soluble FP)$O_{2+x}$ samples which do not contain the simulated metallic inclusions and measured their thermal conductivities to clarify the thermal conductivity changes of oxidized fuel matrix. We also measured thermal conductivities of (U, Gd)$O_{2+x}$ pellets having various O/M ratios to evaluate the effect of oxidation on the thermal conductivity of (U, Gd)$O_2$ pellets. Based on the results of these measurements, we expressed the effect of pellet oxidation on the thermal conductivity of impurity-doped $UO_2$ pellets.

## 2. Experimental

### 2.1. Sample preparation

(U, M)$O_{2+x}$ samples (M = Gd or simulated soluble FPs) were prepared by a method similar to that used to prepare $UO_{2+x}$ samples in our earlier study [7]: disks about 1 mm thick were sliced from (U, M)$O_2$ pellets (M = Gd or simulated soluble FPs) which were sintered at 2023 K for 4 h in $N_2$–8%$H_2$ atmosphere. These disks were oxidized in the conditions summarized in Tables 1 and 2. The O/M ratios of the oxidized samples were calculated from the mass change before and after oxidation and compared with the results determined by a polarography method. The difference in results of deviation from the stoichiometry, $x$, between the two methods was about $\pm 2\%$.

Table 3
Sample characteristics of 10 wt% $Gd_2O_3$ doped $UO_{2+x}$

| O/M ratio | Thickness (mm) | Density (g $cm^{-3}$) | Theoretical density (g $cm^{-3}$) | Porosity (%) |
|---|---|---|---|---|
| 2.00 | 1.505 | 10.32 | 10.64 | 3.0 |
| 2.06 | 1.058 | 10.39 | 10.72 | 3.08 |
| 2.08 | 1.519 | 10.38 | 10.74 | 3.36 |
| 2.11 | 1.505 | 10.43 | 10.78 | 3.25 |
| 2.15 | 1.502 | 10.40 | 10.84 | 4.08 |

Table 4
Sample characteristics of simulated soluble FP-doped $UO_{2+x}$

| O/M ratio | Thickness (mm) | Density (g $cm^{-3}$) | Theoretical density (g $cm^{-3}$) | Porosity (%) |
|---|---|---|---|---|
| (a) Simulated burnup: 30 GW d/t U | | | | |
| 2.00 | 1.010 | 10.43 | 10.83 | 3.69 |
| 2.02 | 1.010 | 10.44 | 10.86 | 3.87 |
| (b) Simulated burnup: 60 GW d/t U | | | | |
| 2.00 | 1.013 | 10.39 | 10.72 | 3.08 |
| 2.02 | 1.013 | 10.40 | 10.76 | 3.35 |

Sample characteristics are shown in Tables 3 and 4. The theoretical density of each sample was evaluated from

its lattice parameter. The phase identifications were carried out by X-ray diffractometry. Only diffraction peaks due to the $UO_{2+x}$ fluorite structure were observed and no peaks for the $M_4O_9$ (M = U + Gd or U + FPs) type structure were seen for (U, M)$O_{2+x}$ samples.

### 2.2. Thermal conductivity measurements

Thermal conductivities of (U, M)$O_{2+x}$ (M = Gd or simulated soluble FPs) were measured by a laser flash method (LF/TCMFA8510SP4, Rigaku). The apparatus and the analysis method have been described elsewhere in detail [12]. The measurements were carried out three times at each temperature step in a vacuum of less than $2 \times 10^{-4}$ Pa. The sample masses were measured before and after the thermal diffusivity measurements and the thermal diffusivity data were accepted only when the sample masses were unchanged. The temperature region with no change of sample mass was from room temperature to 1400 K. The thermal diffusivity of each sample was calculated from its rear-surface temperature response by the 'logarithmic method' [13].

Thermal conductivities of (U, M)$O_{2+x}$ samples (M = Gd or simulated soluble FPs) were estimated from the following equation:

$$\lambda_M = \alpha_M C_p \rho_M, \quad (1)$$

where $\lambda_M$ is the thermal conductivity of the sample, $\alpha_M$ the thermal diffusivity of the sample obtained from thermal diffusivity measurements, $C_p$ the specific heat capacity, and $\rho_M$ the density of the sample.

The specific heat capacities of (U, M)$O_{2+x}$ samples (M = Gd or simulated soluble FPs) were evaluated by using an expression including the non-stoichiometry [14], because the difference between the molar heat capacities of (U, M)$O_{2+x}$ (M = Gd or simulated soluble FPs) calculated from Neumann–Kopp's law and that of $UO_{2+x}$ was small, being about ±2%.

## 3. Results and discussion

### 3.1. Thermal diffusivities of (U, Gd)$O_{2+x}$

The results of thermal diffusivity measurements on (U, Gd)$O_{2+x}$ ($x$ = 0–0.15) are shown in Fig. 1(a). The thermal diffusivity calculated from Ref. [12] is shown in the figure for comparison. The thermal diffusivities were in good agreement for each sample, irrespective of being a heating or cooling process.

### 3.2. Thermal diffusivities of (U, simulated soluble FP)$O_{2+x}$

The results of thermal diffusivity measurements on (U, simulated soluble FP)$O_{2+x}$ ($x$ = 0–0.02, simulated burnups: 30 and 60 GWd/tU) are shown in Fig. 1(b, c). The thermal diffusivities were in good agreement for each sample, irrespective of being a heating or cooling process, similar to $Gd_2O_3$ doped $UO_{2+x}$.

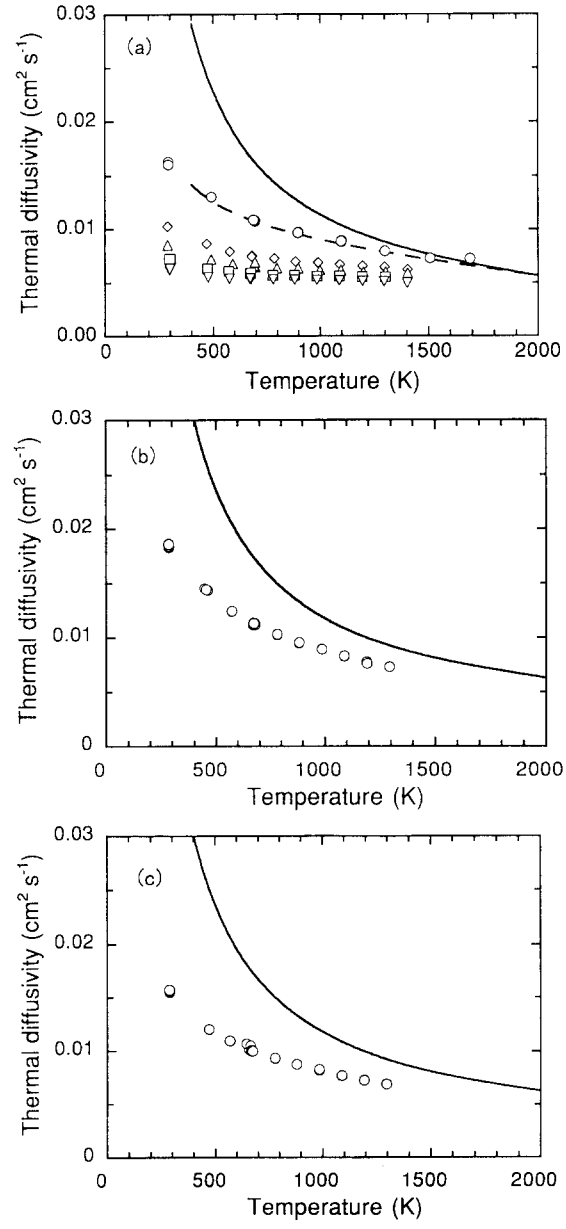


Fig. 1. (a) Thermal diffusivities of 10 wt% $Gd_2O_3$ doped $UO_{2+x}$ pellets. ○: (U, Gd)$O_{2.00}$; ◇: (U, Gd)$O_{2.06}$; △: (U, Gd)$O_{2.08}$; □: (U, Gd)$O_{2.11}$; ▽: (U, Gd)$O_{2.15}$; – – –: (U, Gd)$O_2$ [12]; ————: $UO_2$ [12]. (b) Thermal diffusivities of simulated soluble FP-doped $UO_{2+x}$ pellets (simulated burnup: 30 GWd/tU). ○: (U, FP)$O_{2.02}$; ————: $UO_2$ [12]. (c) Thermal diffusivities of simulated soluble FP doped $UO_{2+x}$ pellets (simulated burnup: 60 GWd/tU). ○: (U, FP)$O_{2.02}$; ————: $UO_2$ [12].

### 3.3. Thermal conductivities of (U, M)$O_{2+x}$ (M = Gd or simulated soluble FPs)

Fig. 2(a–c) plot the thermal conductivities of (U, M)$O_{2+x}$ (M = Gd or simulated soluble FPs) pellets evaluated from Eq. (1). Thermal conductivity of each sample was normalized to that with 96.5% of the theoretical density (TD) by applying a modified Loeb's equation:

$$\lambda_{96.5} = \{(1 - 0.035\beta)/(1 - \beta P)\}\lambda_M, \quad (2)$$

where $\lambda_{96.5}$ is the thermal conductivity of the sample normalized to 96.5% TD, $\beta$ a coefficient, $P$ the porosity of the sample, and $\lambda_M$ the measured thermal conductivity of the sample. The value of $\beta$ was assumed to be the same as for $UO_2$ [15]:

$$\beta = 2.6 - 5 \times 10^{-4}(T - 273.15), \quad (3)$$

where $T$ is the temperature in K.

As shown in Fig. 2(a–c), the thermal conductivities of (U, M)$O_{2+x}$ decreased as the deviation from the stoichiometric composition, $x$, increased. The break points of the thermal conductivities which were observed for $UO_{2+x}$ due to the phase transition [7] were not observed for (U, M)$O_{2+x}$. Therefore, the $M_4O_9$–$MO_2$ (M = U + Gd or U + FPs) mixture phase may not exist even at room temperature in (U, M)$O_2$. This would be in agreement with the phase identification results by X-ray diffraction.

In general, phonon–phonon scattering (Umklapp process) and phonon-impurity (substitutional impurity) scattering are dominant mechanisms of heat resistance in ceramics above room temperature. Klemens [8,9] has proposed a heat conduction model in materials when phonon–phonon scattering and phonon-impurity scattering occur simultaneously. According to this model, the thermal conductivity of the crystal lattice in vibration $\lambda_P$ is expressed as

$$\lambda_P = \lambda_0 \tan^{-1}(\theta)/\theta, \quad (4)$$

$$\theta = S\sqrt{\Gamma\lambda_0}, \quad (5)$$

where $\lambda_0$ is the thermal conductivity of impurity-free material, $\theta$ the phonon scattering parameter by the impurity, $S$ a coefficient, and $\Gamma$ a parameter expressed as

$$\Gamma = \sum_i y_i\left[(\Delta M_i/M)^2 + \xi(\Delta r_i/r)^2\right]. \quad (6)$$

Here $y_i$ is the atomic partial ratio of the impurity, $M$ the mean mass, $r$ the mean ionic radius, $\Delta M_i$ the mass difference between the impurity and matrix atoms, $\Delta r_i$ the ionic radius difference between the impurity and matrix atoms, and $\xi$ a coefficient.

In the (U, M)$O_{2+x}$ (M = Gd and/or simulated soluble FPs) crystal lattice, the excess oxygen atoms exist in interstitial positions and in order to maintain the electrical neutrality, $U^{5+}$ ions must be present in the (U, M)$O_{2+x}$ crystal lattice.

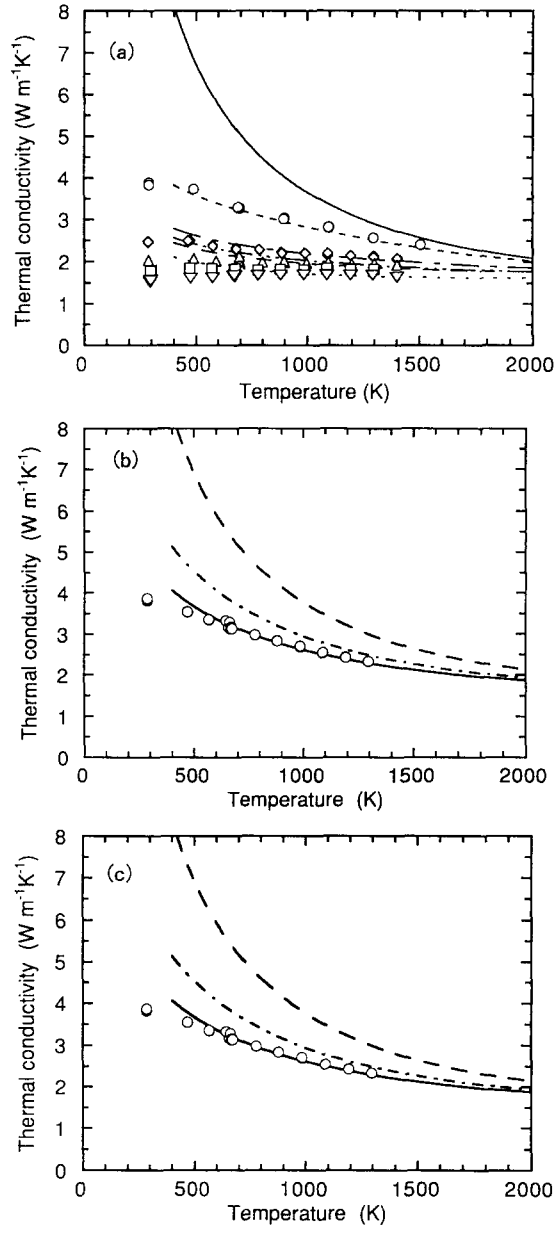


Fig. 2. (a) Thermal conductivities of 10 wt% $Gd_2O_3$ doped $UO_{2+x}$ pellets. Symbols: measured values, lines: calculated values from Eq. (10). ○: (U, Gd)$O_{2.00}$; ◇: (U, Gd)$O_{2.06}$; △: (U, Gd)$O_{2.08}$; □: (U, Gd)$O_{2.11}$; ▽: (U, Gd)$O_{2.15}$; ————: $UO_2$ [17]; ---: (U, Gd)$O_2$ [16]; — — —: (U, Gd)$O_{2.06}$; — · — · —: (U, Gd)$O_{2.08}$; — — —: (U, Gd)$O_{2.11}$; · · · : (U, Gd)$O_{2.15}$. (b) Thermal conductivities of simulated soluble FP-doped $UO_{2+x}$ pellets (simulated burnup: 30 GWd/tU). ○: (U, FP)$O_{2.02}$; ————: (U, FP)$O_{2.02}$; — — —: (U, FP)$O_2$ [17]; — · — · —: $UO_2$ [16]. (c) Thermal conductivities of simulated soluble FP-doped $UO_{2+x}$ pellets (simulated burnup: 60 GWd/tU). ○: (U, FP)$O_{2.02}$; ————, (U, FP)$O_{2.2}$; — — —: (U, FP)$O_2$ [17]; — · — · —: $UO_2$ [16].

From the thermal conductivity analyses of $Gd_2O_3$ [16] and/or simulated FP-doped $UO_2$ [17] and $UO_{2+x}$ [7], the phonon scattering parameter, $\theta$, is nearly proportional to the square root of the concentrations of $Gd^{3+}$ and/or simulated FP and $U^{5+}$ ions. Then, the following equation was assumed to hold:

$$\theta_i = [D_i y_i \lambda_0]^{1/2}, \tag{7}$$

where $\theta_i$ is the phonon scattering parameter of impurity $i$ ($i = Gd^{3+}$, simulated FP ions and $U^{5+}$), $D_i$ a coefficient which expresses the effect of impurity $i$, and $y_i$ the atomic concentration of impurity $i$.

According to Klemens' theory [8,9] based on the relaxation process of phonon scattering, the phonon scattering parameter, $\theta$, is proportional to the square root of the phonon scattering probability in the crystal lattice containing impurity. The phonon scattering probability by impurities in the (U, M)$O_2$ (M = Gd and/or simulated soluble FPs) crystal lattice is expressed as follows using the phonon mean free path:

$$1/l_p = 1/l_M + 1/l_{O/U}, \tag{8}$$

where $l_p$ is the phonon scattering mean free path in (U, M)$O_{2+x}$, $l_M$ is that in (U, M)$O_2$, and $l_{O/U}$ is that in $UO_{2+x}$. Therefore, the phonon scattering parameter $\theta$ is expressed as

$$\theta^2 = \theta_M^2 + \theta_{O/U}^2, \tag{9}$$

where $\theta$ is the phonon scattering parameter of (U, M)$O_{2+x}$, $\theta_M$ is that of (U, M)$O_2$ and $\theta_{O/U}$ is that of $UO_{2+x}$. Fig. 3 compares the measured phonon scattering parameters evaluated from the thermal conductivities and those calculated with Eq. (9) using our previous results of $\theta_M$ and $\theta_{O/U}$ [7,16,17]. The measured values showed fairly good agreement with the calculated values and the phonon scattering parameter could be expressed using the summation rule among the phonon scattering parameters of $Gd^{3+}$ ions, soluble FP ions and $U^{5+}$ ions. The coefficients $D_M$ (M = Gd and/or simulated soluble FPs) and $D_{O/U}$ were obtained in our previous studies [7,16,17]. Using these values, we formulated the thermal conductivity of (U, M)$O_{2+x}$ (M = Gd and/or simulated soluble FPs) for 96.5% TD as

$$\lambda = \lambda_0\{\tan^{-1}(\theta)/\theta\} + CT^3 \ (\mathrm{W\ m^{-1}\ K^{-1}}), \tag{10}$$

where $\lambda_0 = 1/(A + BT)$, $\theta = [D_{Gd}^2 y_{Gd}\lambda_0 + D_{FP}^2 y_{FP}\lambda_0 + D_{O/U}^2(2x)\lambda_0]^{1/2}$, $A = 3.24 \times 10^{-2}$ (m K $W^{-1}$), $B = 2.51 \times 10^{-4}$ (m $W^{-1}$), $C = 5.91 \times 10^{-11}$ (W $m^{-1}$ $K^{-4}$), $D_{Gd} = D_{0,Gd}\exp(D_{1,Gd}T)$ ($m^{1/2}$ $K^{1/2}$ $W^{-1/2}$), $D_{FP} = D_{0,FP}\exp(D_{1,FP}T)$ ($m^{1/2}$ $K^{1/2}$ $W^{-1/2}$), $D_{O/U} = D_{0,O/U}\exp(D_{1,O/U}T)$ ($m^{1/2}$ $K^{1/2}$ $W^{-1/2}$), $D_{0,Gd} = 3.24$ ($m^{1/2}$ $K^{1/2}$ $W^{-1/2}$), $D_{1,Gd} = -7.92 \times 10^{-4}$ ($K^{-1}$), $D_{0,FP} = 2.81$ ($m^{1/2}$ $K^{1/2}$ $W^{-1/2}$), $D_{1,FP} = -1.63 \times 10^{-4}$ ($K^{-1}$), $D_{0,O/U} = 3.67$ ($m^{1/2}$ $K^{1/2}$ $W^{-1/2}$), $D_{1,O/U} = -4.73 \times 10^{-4}$ ($K^{-1}$), $y_{Gd}$ is the atomic concentration of Gd, $y_{FP}$ the atomic concentration of soluble FPs, $x$ the deviation from stoichiometry, and $T$ the temperature (K).

The values calculated by Eq. (10) are compared with the measured ones in Fig. 2(a–c). Eq. (10) can express the thermal conductivity of (U, M)$O_2$ (M = Gd or simulated soluble FPs) fairly well in the temperature region above 700 K. Below 700 K, the thermal conductivity calculated from Eq. (10) tends to be higher than the measured value. The difference between them could not be explained, but may be because of a Willis' (2:1:2) or (2:2:2) cluster which may exist in the (U, M)$O_{2+x}$ solid solution [18,19]: the clusters may affect the thermal conductivity of ceramics in lower temperature region than point defects do [20].

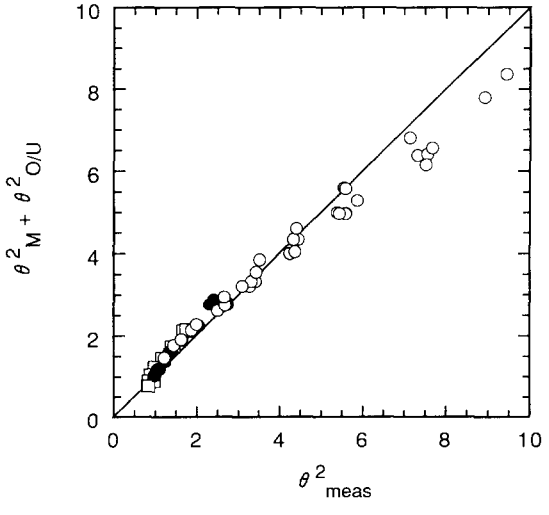


Fig. 3. Squared measured phonon scattering parameter, $\theta^2_{meas}$, as a function of the calculated values using $\theta^2_M$ (M = Gd or simulated soluble FPs) and $\theta^2_{O/U}$ from Eq. (9). ○: (U, Gd)$O_{2+x}$; ●: U, FP)$O_{2+x}$ (simulated burnup: 30 GWd/tU); □: (U, FP)$O_{2+x}$ (simulated burnup: 60 GWd/tU); ————: $\theta^2_{meas} = \theta^2_M + \theta^2_{O/U}$ (M = Gd or simulated soluble FPs).

### 3.4. Comparison between literature data and calculated values

Lucuta et al. [6] measured the thermal conductivities of unirradiated hyperstoichiometric SIMFUEL (simulated burnups: 3.0 and 8.0 at.%). The values calculated from our expression (Eq. (10)) are compared with their values in Figs. 4 and 5.

The calculated values were in fairly good agreement with the literature data above 1000 K. On the other hand, the literature data tended to be higher than the values calculated from Eq. (10) below 1000 K except for 8 at.% burnup.

The difference between the literature data and the calculated values may be mainly due to the following two reasons: (1) the effects of simulated metallic inclusions and/or (2) the precipitations of $M_4O_9$ phase similar to $U_4O_9$ phase, which may form heat paths in pellets similar to $UO_{2+x}$ [4,7].

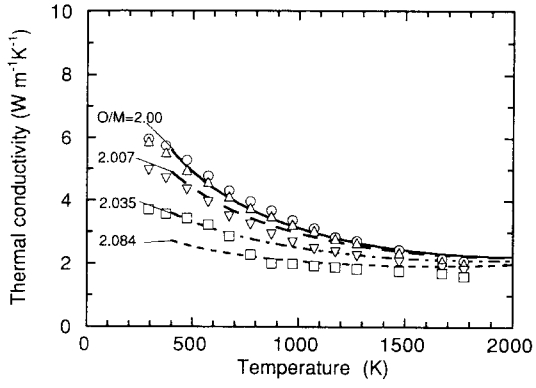


Fig. 4. Comparison between calculated values and literature data [6] (simulated burnup: 3 at.%). Lines: calculated from Eq. (10), symbols: from Lucuta et al. [6]. ————, ○: O/M = 2.00; – – –, △: O/M = 2.007; — — —, ▽: O/M = 2.035; ---, □: O/M = 2.084.

The effects of simulated metallic inclusions have already been estimated by Lucuta et al. for stoichiometric SIMFUELs [21] and the contribution of metallic inclusions was about 1% increase in the thermal conductivity for each 1 at.% burnup. In consideration of this result and the fact that our calculated values agreed well with the literature data above 1000 K in spite of ignoring metallic inclusion in the calculation, the effect of metallic inclusions on the thermal conductivity of hyperstoichiometric SIMFUEL may be neglected in the temperature region of our studies.

Lucuta et al. [6] mentioned only that the $U_4O_9$ phase was not observed for hyperstoichiometric 8 at.% burnup SIMFUEL and for the hyperstoichiometric 3 at.% burnup SIMFUEL annealed at the lower oxygen potentials from their X-ray diffraction results. Therefore, the disagreement between the literature data and our calculated values in the low temperature region for the 3 at.% burnup SIMFUEL

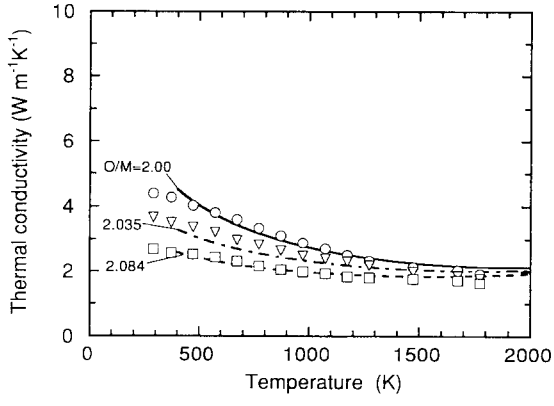


Fig. 5. Comparison between calculated values and literature data [6] (simulated burnup: 8 at.%). Lines: calculated from Eq. (10); symbols: Lucuta et al. [6]. ————, ○: O/M = 2.00; — — —, ▽: O/M = 2.035, ---, □: O/M = 2.084.

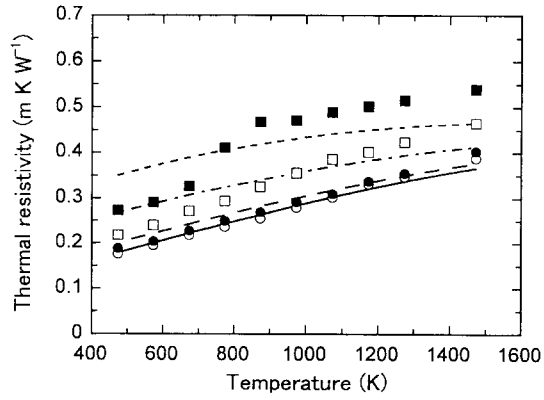


Fig. 6. Thermal resistivities of hyperstoichiometric SIMFUEL (simulated burnup: 3.0 at.%). Symbols: thermal resistivities re-calculated from the data of Lucuta et al. [6]; lines: thermal resistivities calculated from Eq. (10). ————, ○: O/M = 2.00; – – –, ●: O/M = 2.007; — — —, □: O/M = 2.035; ---, ■: O/M = 2.084.

having O/M = 2.084 may be mainly due to the effects of precipitation of the $M_4O_9$ phase.

In order to investigate the effects of $M_4O_9$ phase on the thermal conductivity of hyperstoichiometric 3 at.% burnup SIMFUEL in detail, we re-calculated the thermal resistivities from the thermal conductivity data of Lucuta et al. [6]. The results were shown in Fig. 6. The thermal resistivities calculated from our formula (Eq. (10)) were also shown for comparison. Fig. 7 shows the deviation of the thermal resistivity data from the lines from our expression in Fig. 6. The tendency of the deviation for O/M = 2.007 were similar to that of unoxidized 3 at.% burnup SIMFUEL. Therefore, the sample having O/M = 2.007 may not contain the precipitates of $M_4O_9$ phase and the thermal conductivities may not be affected by the $M_4O_9$ precipitates. On the other hand, the behavior of deviation for O/M =

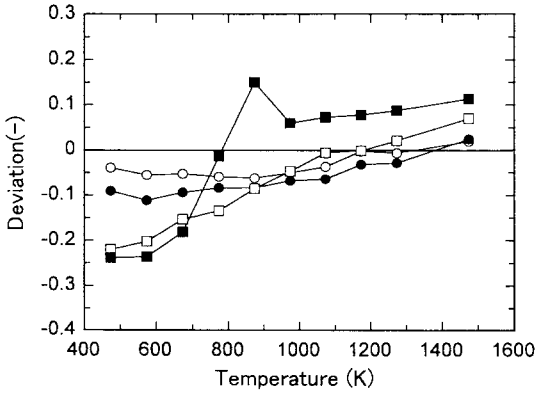


Fig. 7. Deviation of the measured thermal resistivities from the lines in Fig. 6 (simulated burnup: 3.0 at.%). Symbols: thermal resistivities re-calculated from the data of Lucuta et al. [6].

2.035 in Fig. 7 was similar to that for O/M = 2.084 rather than that for unoxidized one in the low temperature region. This indicates the thermal resistivities for O/M = 2.035 may contain the effects of the $M_4O_9$ precipitates, which was probably not identified by X-ray diffraction analysis. The thermal conductivities of 3 at.% burnup SIMFUEL having O/M = 2.035 tend to be higher than our calculated values below 1000 K. The difference between our calculated values and the Lucuta et al.'s data for O/M = 2.035 in the low temperature region may be mainly due to the precipitation of $M_4O_9$ phase.

## 4. Conclusion

Thermal diffusivities of (U, M)$O_{2+x}$ (M = Gd or simulated soluble FPs) were measured by a laser-flash method from room temperature to 1400 K. Thermal conductivities of (U, M)$O_{2+x}$ decreased as their hyperstoichiometry, $x$, increased. The concentration of $U^{5+}$ ion formed due to excess interstitial oxygen in relation to Klemens' equation led to the expression of $\lambda$, the thermal conductivity of (U, M)$O_{2+x}$ (M = Gd and/or simulated soluble FPs) pellets for 96.5% TD, as a function of their hyperstoichiometry $x$, impurity content $y$ and temperature in K, given in Eq. (10).

The values calculated by Eq. (10) were in fairly good agreement with the measured values for 10 wt% $Gd_2O_3$ doped $UO_{2+x}$ ($0 \leq x \leq 0.15$) and simulated soluble FP doped $UO_{2+x}$ ($0 \leq x \leq 0.02$, simulated burnup: 30 and 60 GWd/tU) in the temperature region above 700 K. Below 700 K, the thermal conductivity calculated from the above formula tends to be higher than the measured value. The tendency may be due to the defect clusters of oxygen atoms such as a Willis' (2:1:2) or (2:2:2) cluster.

## Acknowledgements

The authors would like to express their gratitude to Dr K. Une for valuable discussions. They also thank Mr H. Masuda for sample preparation and Mr Y. Okoshi for sample composition analysis.

## References

[1] K. Une, M. Imamura, M. Amaya, Y. Korei, J. Nucl. Mater. 223 (1995) 40.
[2] A. M. Ross, USAEC Reports, CRFD-817, AECL-1096, 1960.
[3] V.C. Howard, T.F. Gulvin, U.K.A.E.A IG Rpt. 51 (Rd/C), 1960.
[4] L.A. Goldsmith, J.A.M. Douglas, J. Nucl. Mater. 47 (1973) 31.
[5] I.C. Hobson, R. Taylor, J.B. Ainscough, J. Phys. D7 (1974) 1003.
[6] P.G. Lucuta, Hj. Matzke, R.A. Verrall, J. Nucl. Mater. 223 (1995) 51.
[7] M. Amaya, T. Kubo, Y. Korei, J. Nucl. Sci. Technol. 33 (1996) 636.
[8] P.G. Klemens, Proc. Phys. Soc. A68 (1955) 1113.
[9] P.G. Klemens, Phys. Rev. 119 (1960) 507.
[10] K. Une, M. Oguma, J. Nucl. Sci. Technol. 20 (1983) 844.
[11] P.G. Lucuta, R.A. Verrall, Hj. Matzke, B.J.F. Palmer, J. Nucl. Mater. 178 (1990) 48.
[12] M. Hirai, J. Nucl. Mater. 173 (1990) 247.
[13] Y. Takahashi, I. Yamamoto, T. Ohsato, Netsu-Sokutei 15 (1988) 103.
[14] D.L. Hagrman, G.A. Reyman, eds., TREE-NUREG-CR-0497, 1979.
[15] R. Brandt, G. Neuer, J. Non-Equilib. Thermodyn. 1 (1976) 3.
[16] M. Hirai, S. Ishimoto, J. Nucl. Sci. Technol. 28 (1991) 995.
[17] S. Ishimoto, M. Hirai, K. Ito, Y. Korei, J. Nucl. Sci. Technol. 31 (1994) 796.
[18] B.T.M. Willis, J. Phys. (Paris) 25 (1964) 431.
[19] T. Fujino, Nippon Kinzoku Gakkai Kaihou 29 (1990) 71.
[20] P.G. Klemens, G.F. Hurley, F.W. Clinard Jr., Proc. 2nd Topical Meeting. Tech. Controlled Nucl. Fusion, Am. Nucl. Soc., -ERDA-, EPRI, 4 Vols., Conf-760935, 1976.
[21] P.G. Lucuta, Hj. Matzke, R.A. Verrall, J. Nucl. Mater. 217 (1994) 279.